Freely Suspended Layer-by-Layer Nanomembranes: Testing Micromechanical Properties**

By *Sergiy Markutsya*, *Chaoyang Jiang*, *Yuri Pikus*, and *Vladimir V. Tsukruk**

Freely suspended nanocomposite layer-by-layer (LbL) nanomembranes composed of a central layer of gold nanoparticles sandwiched between polyelectrolyte multilayers are fabricated via spin-assisted LbL assembly. The diameter of the circular membranes is varied from 150 to 600 μm and the thickness is kept within the range of 25–70 nm. The micro- and nanomechanical properties of these membranes are studied using a combination of resonance-frequency and bulging tests, and point-load nanodeflection experiments. Our results suggest that these freely suspended nanomembranes, with a Young's modulus of 5–10 GPa are very robust and can sustain multiple significant deformations. They are very sensitive to minor variations in pressure, surpassing ordinary semiconductor and metal membranes by three to four orders of magnitude and therefore have potential applications as pressure and acoustic microsensors.

1. Introduction

During the last decade, the fast development of microelectromechanical systems (MEMS)[1] was ignited by broad interests related to prospective applications of different microdevices, including micromotors, microfluidic switches, and microsensors.[2–6] The prospective use of MEMS as pressure, thermal, and acoustic microsensors has also been pursued in a quest to miniaturize current centimeter-sized devices. In such systems, freely suspended inorganic membranes are used as a sensing element or an actuator for transferring the mechanical deflections to electrical signals and vice versa. These membrane sensing elements are usually manufactured from silicon, ceramic, or carbon[7,8] and have high sensitivity and low noise if their dimensions are kept within the centimeter range. These membranes have a high sensitivity due to their low flexural rigidity caused by an overwhelming contribution from the membrane diameter in the form Eh/a^4 (where E is the elastic modulus, h is the thickness, and a is the diameter of the membrane). Recently, a lithographical approach to membrane-based MEMS was used and a fairly high sensitivity was demonstrated for membranes with diameters in the millimeter range.[9] However, attempts to scale down these membranes to the microscale face a critical challenge directly related to diminishing sensitivity because another ten-fold decrease in membrane diameter (e.g., from millimeters to hundreds of microns) would result in a 10^4 increase in flexural rigidity. The possible decreases in thickness and elastic modulus are severely limited by the choice of material and the resolution of the lithographical technique. Thus, the conventional membranes become exceedingly stiff and quickly lose their sensitivity.

As an alternative route to compliant membranes, polymers, liquid crystals, and lipids have been widely used.[10–13] However, these membranes are usually very fragile and cannot sustain the disturbances that are important for demanding applications, such as mechanically responsive sensors with significant mechanical stresses. Mechanically robust, free-standing, compliant membranes have been synthesized by crosslinking amphiphilic Langmuir[13,14] and cast films.[15] Recently, there have also been reports on the fabrication of a freely suspended membrane using conventional layer-by-layer (LbL) assembly (widely used for a variety of materials)[16–21] combined with sacrificial or pH-sensitive substrates.[22,23] However, all these approaches are very time-consuming, with the sample preparation taking several hours (even days) and requiring multiple stages. The final membranes are frequently very fragile. To overcome these problems, relatively thick (a fraction of a micrometer) membranes are usually fabricated.

We have suggested using spin-assisted layer-by-layer (SALbL) assembly as an alternative, time-efficient fabrication approach to free-standing or freely suspended nanocomposite membranes.[24–26] SALbL assembly has been introduced independently by two research groups.[27,28] This fabrication method combines the very well known spin-coating technique[29] with conventional LbL assembly,[30] making the LbL assembly more simple, time-efficient, and cost-effective. Spin-coating is a standard technique in industry for preparing thin films for different applications, such as gas sensing[31] and light emission,[32] and SALbL assembly can also be easily utilized. We fabricated polyelectrolyte multilayered films containing gold nanoparticles and studied the collective surface plasmon resonances of gold nanoparticles.[24] Free-standing, nanoscale multilayered films with thickness well below 100 nm have been obtained using SALbL combined with the sacrificial-layer method intro-

[*] Prof. V. V. Tsukruk, S. Markutsya, Dr. C. Jiang, Dr. Y. Pikus
Department of Materials Science and Engineering
Iowa State University
Ames, IA 50011 (USA)
E-mail: vladimir@iastate.edu

[**] This work was supported by the NSF, Grant CTS-0210005 and the AFOSR, Grant F496200210205. We thank H. Shulha, X. Tan, and A. Bastawros, Iowa State University, and M. R. Begley, University of Virginia for valuable discussions. TEM investigations were done with the kind help of F. Laabs and M. Kramer from Ames Laboratory.

DOI: 10.1002/adfm.200400149

duced by Kotov.[22] Initial testing of micromechanical properties of these nanoscale membranes demonstrated their high robustness, toughness, and mechanical strength.

Herein, we report further studies on these robust, compliant, and highly sensitive SALbL nanomembranes with outstanding mechanical stability. The micro- and nanomechanical properties of the nanocomposite membranes, composed of a central layer containing gold nanoparticles sandwiched between polymer multilayers, were studied using resonance-frequency and bulging tests, and the point-load proximity probe method. Critical micromechanical characteristics, such as elastic moduli, residual stresses, and deflection mechanisms were investigated for these membranes. We demonstrated that nanomembranes with overall thicknesses ranging from 25 to 70 nm suspended over circular openings 150 to 600 μm in diameter combined high mechanical stability with outstanding pressure sensitivity, making them excellent candidates for highly sensitive acoustic sensors.

2. Results and Discussion

2.1. Fabrication of Nanocomposite Membranes

To fabricate freely suspended, multilayered nanocomposite membranes containing gold nanoparticles, we used SALbL assembly according to the procedures originally described.[27,28] The sacrificial-layer technique was used to release a multilayered polymer film from the substrate in accordance with the original procedure.[22,23] The gold nanoparticles were deposited on n bilayers of oppositely charged polyelectrolytes, followed by covering with an additional n bilayers (Fig. 1a). Conventional polyelectrolytes (Fig. 1b), poly(sodium 4-styrene sulfonate), PSS, and poly(allylamine hydrochloride), PAH, were used as the negatively and positively charged counterparts, respectively (see Experimental). The multilayered polymer films with gold nanoparticles were released from the supporting silicon wafer by dissolving a sacrificial cellulose acetate (CA) layer in acetone (Fig. 1a). The freely suspended membrane was transferred to a water surface, then lifted using a highly polished copper holder with a carefully micromachined central hole, 150, 400, or 600 μm in diameter. The freely suspended membranes on the copper holder were stored in a sealed container before and between measurements. The general scheme of the freely suspended nanocomposite membranes, shown in Figure 2, can be traditionally represented by a general formula $(PAH/PSS)_n$/PAH/Au/$(PAH/PSS)_n$/PAH [or in a simpler form as n/Gold/n (nGn)] where n represents the number of PAH/PSS bilayers in the polymer portions of the membrane (Fig. 2). The number of the bilayers tested here varied from three to eleven.

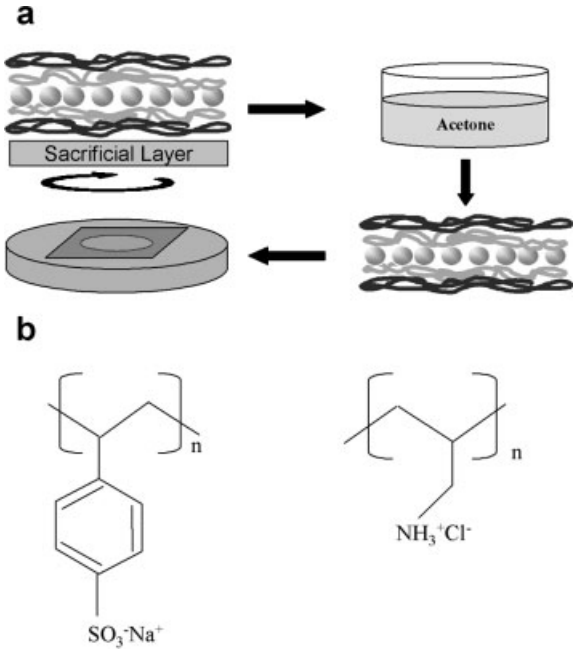

Figure 1. a) Scheme of the SALbL membrane fabrication and release. b) Chemical structures of the polymers, PSS (left) and PAH (right).

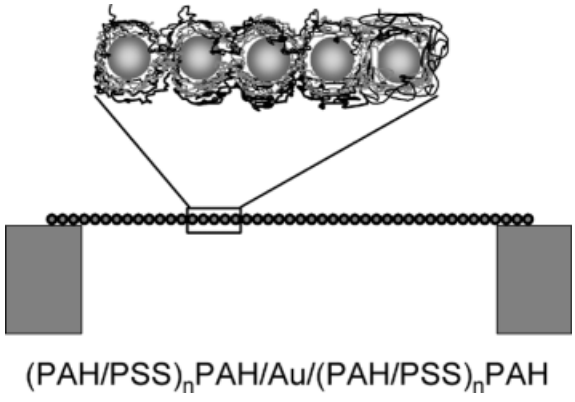

Figure 2. General schematic of the freely suspended membrane and the microstructure of the freely suspended membrane with a central gold-nanoparticle monolayer sandwiched between two symmetrical polyelectrolyte multilayers ($n = 3$) and the general formula for the multilayered nanomembranes.

2.2. Membrane Microstructure and Morphology

A detailed discussion of the SALbL membrane surface morphology and microstructure has been published elsewhere[24,25] and herein we briefly summarize the major points that are important for understanding the micromechanical properties. The gold nanoparticles deposited on the oppositely charged polymer layer were uniformly distributed in the membrane, as was confirmed via both transmission electron microscopy (TEM) and atomic force microscopy (AFM) (Fig. 3). The TEM images were collected directly for a freely suspended membrane on a 200-mesh copper grid. From the higher magnification TEM image (Fig. 3b), individual nanoparticles can be clearly observed. The diameter distribution of the gold nanoparticles was obtained by measuring the diameter of 200 nanoparticles in the TEM image. Figure 3d shows the histogram of diameter distribution for the gold nanoparticles: The average diameter was 12.7 ± 1.3 nm, which is very close to the diameter measured from the AFM images (Fig. 3c) discussed elsewhere.[24] In this study, the surface coverage of gold nanoparticles varied from 25 to 30 %.[24]

ADVANCED FUNCTIONAL MATERIALS

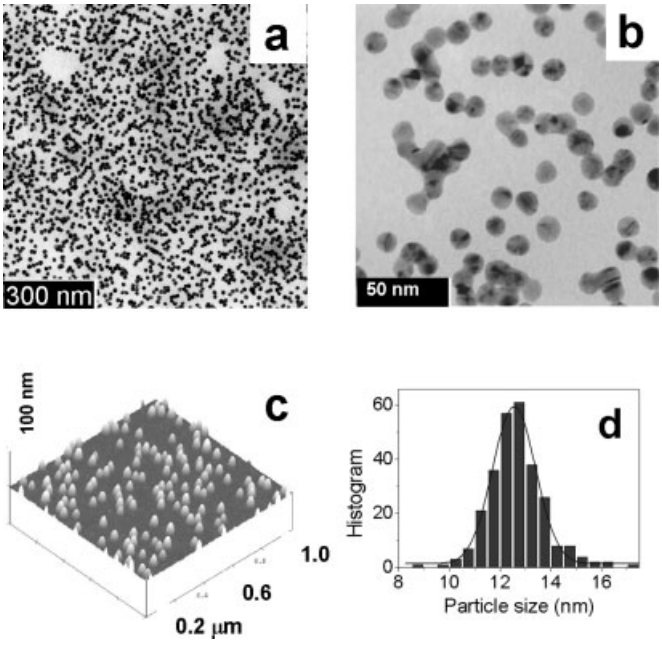

Figure 3. a) TEM image of a freely suspended 9G9 membrane; note that the uniformity of the distribution of the gold nanoparticles. b) Higher-magnification TEM image of the 9G9 membrane, note the randomly distributed and isolated gold nanoparticles. c) Three-dimensional AFM topographical image of low-concentration gold nanoparticles on a PAH monolayer. d) Diameter distribution of the gold nanoparticles: an average diameter of 12.7 ± 1.3 nm was obtained from the TEM data analysis.

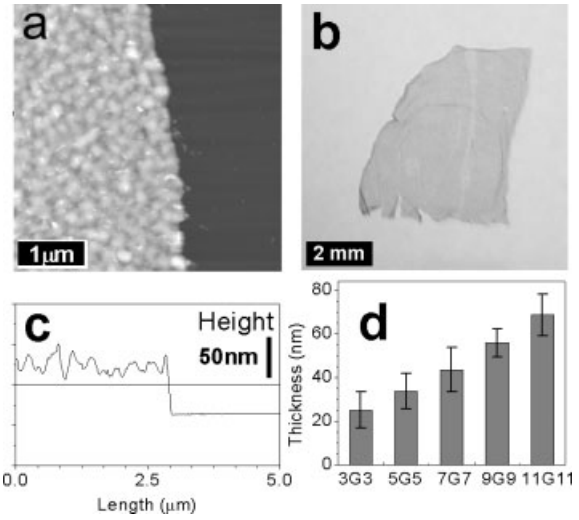

Figure 4. a) AFM image of the edge of a free-standing membrane picked up onto a silicon substrate. b) Optical microscope image of a freely suspended membrane floating on a water surface. c) Cross-section of the membrane edge. d) The thickness of the *n*G*n* membranes with different number of bilayers, *n*.

The thickness of the membranes could easily be tuned in the range from 30 to 100 nm by varying the number of polymer bilayers n, in increments of 2.7 nm, which represents the average thickness of the bilayer, as was independently determined from ellipsometric and AFM thickness measurements. The nanocomposite membranes, with typical lateral dimensions of about 5 mm × 5 mm can float on a water surface and were easily picked up using the copper holder. The membranes have relatively smooth surfaces, with a microroughness within 1×1 μm^2 not exceeding 8 nm, and a low concentration of wrinkles and cracks.

The membranes' thicknesses were measured along the edges of freely suspended membranes transferred onto silicon wafers from a water surface (Fig. 4). From this analysis, the thickness of freely suspended *n*G*n* membranes, with $n = 3$, 5, 7, 9, and 11, were measured and the results of these measurements are combined in Figure 4d. These data clearly demonstrate that the thickness of the *n*G*n* membranes increases linearly with the number of PAH–PSS bilayers, and is a good indication of the multilayered structure of these membranes as suggested for conventional LbL films.[30] Extrapolation of the this plot to zero layers yields an extrapolated thickness below the nanoparticle diameter. This suggests that at first several polymeric layers are deposited predominantly in the gaps among the gold nanoparticles, with further layers being more uniformly distributed. The mechanical testing reported herein was performed on a 9G9 membrane with a relatively uniform surface morphology. (Similar results were obtained for the 7G7 membrane.) Membranes with fewer polymeric layers showed lower mechanical properties, as will be discussed in future publications.

2.3. Micromechanical Properties from Resonance-Frequency Testing

Resonance-frequency measurements of freely suspended nanomembranes were used to estimate their nanomechanical properties under dynamic conditions of fast vibrations with nanoscale amplitude. The resonance amplitude of the freely suspended nanomembranes depended linearly upon the drive amplitude, and varied from 5 to 30 nm, as demonstrated in Figure 5. According to these results, all nanocomposite membranes showed a very stable resonant behavior at high frequencies (e.g., about 100 kHz for the 400 μm diameter membrane, as shown in Fig. 5). The quality factor Q[33,34] calculated from the resonance-frequency data characterizes the damping properties of the membranes, and was relatively high considering the large surface area of the membranes. For a 9G9 membrane 400 μm in diameter, the Q factor reached 80—compared to typical values of above 100 for stiff, inorganic membranes.[35] This value decreased for larger-diameter membranes and increased for smaller membranes, as expected for such structures.[34]

From resonance-frequency measurements, the elastic modulus of the membranes was evaluated using the known formula for the resonance frequency, f_0, of a circular uniform plate clamped at the edges (Eq. 1):[36]

$$f_0 = \frac{\alpha}{a^2\sqrt{1+\beta}}\sqrt{\frac{gD}{\rho h}} \quad (1)$$

where a is the radius of membrane, $D = (Eh^3)/[12(1-\nu^2)]$ is the flexural rigidity of the membrane (E is the elastic modulus, ν is

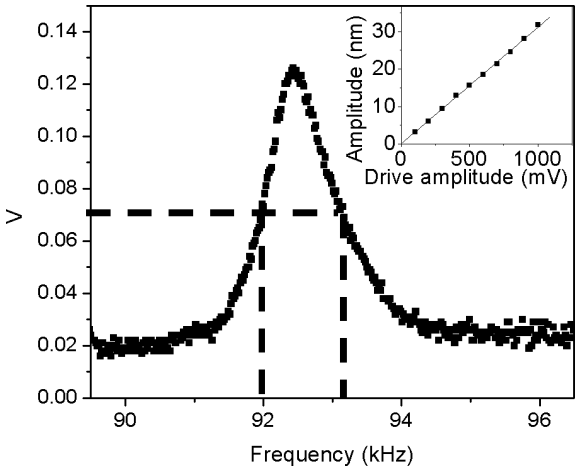

Figure 5. The resonance peak for a freely suspended 9G9 membrane 400 μm in diameter. The dashed horizontal line shows half the amplitude of the resonance peak. The two vertical dashed lines show the half-width. Inset: variation of the membrane amplitude [nm] with the piezotube driving amplitude.

Poisson's ratio), ρ is the density of the membrane, h is the thickness of the membrane, $\beta = 0.6689\ (\rho_1/\rho)(a/h)$ is the correction coefficient that takes into account the density of the air ρ_1, and α is a constant that corresponds to the appearance of the nodal lines during vibrations.

In our calculations, α was 39.78, which corresponds to the vibration mode with one nodal circle. The Poisson ratio was taken as 0.3, which is a typical value for polymeric materials below their glass-transition temperature.[36,37] This vibration mode was selected in accordance with preliminary bulging results, and to give a reasonable estimate of the elastic modulus of the polymer membranes. A high temporal stability of the membranes under high frequencies was observed during these measurements. From these experiments, the elastic moduli for the freely suspended membranes with different diameters were found to be in the range 12 to 15 GPa (Table 1). However, we used these values only as preliminary estimates, because the presence of a number of secondary resonances in our experimental set-up prevented us from conducting more sophisticated measurements and analysis for these membranes. Two other independent tests, bulge testing and stress–strain experiments, provided more reliable data on the micromechanical properties.

Table 1. Elastic moduli for 9G9 membranes of different diameters, calculated from the resonance-frequency test (E_1), bulging test fitting (E_2), and from stress–strain curves (E_3), in comparison with the composite modulus calculated using the Takayanagi model (E_T); and residual stresses.

Diameter [μm]	E_1 [GPa]	E_2 [GPa]	E_3 [GPa]	E_T calculated	Residual stress [MPa]
600	12.3	6.6 ± 2.3	6.4 ± 2.2	7.2	14.3 ± 3.1
400	12.1	9.6 ± 2.5	9.0 ± 2.4	7.2	20.7 ± 12.5
150	15.4	5.7 ± 3.0	5.7 ± 3.0	7.2	15.0 ± 5.4

2.4. Micromechanical Properties from Bulging Experiments

The micromechanical properties of the compliant membranes could be studied in the range of regimes with the well-known bulging technique.[38,39] In a bulging test, a micromechanical response is measured as a deflection of the membrane subjected to overpressure. The deflection over a wide range—from tens of nanometers to tens of micrometers—can be measured with the optical interference set-up system shown in Figure 6. The distance between two rings of the same color corresponds to the half of the wavelength distance in the z-direction. A detailed analysis of the shape of the membranes and its behavior under variable pressure allows the stress–strain behavior, elastic modulus, and residual stress to be estimated according to known procedures.[39]

In fact, the deflected membranes give rise to different interference patterns under variable pressure (Fig. 7). The membrane in the resting state (Fig. 7a) displays a fluctuating interference pattern, reflecting random deflections within several hundred nanometers due to external acoustic noise. Applying an external pressure to the membrane resulted in a series of concentric Newton rings, which increased in number for higher pressures (Figs. 7b–d). For modest deflections, the spacing of the rings is very uniform and the number of rings is proportional to its square radius (Fig. 8a). This result confirms the

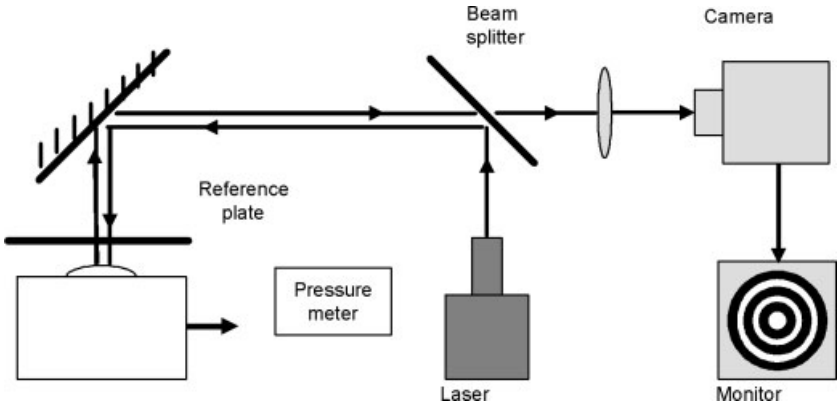

Figure 6. Scheme of the custom-built interferometry set-up.

ADVANCED FUNCTIONAL MATERIALS

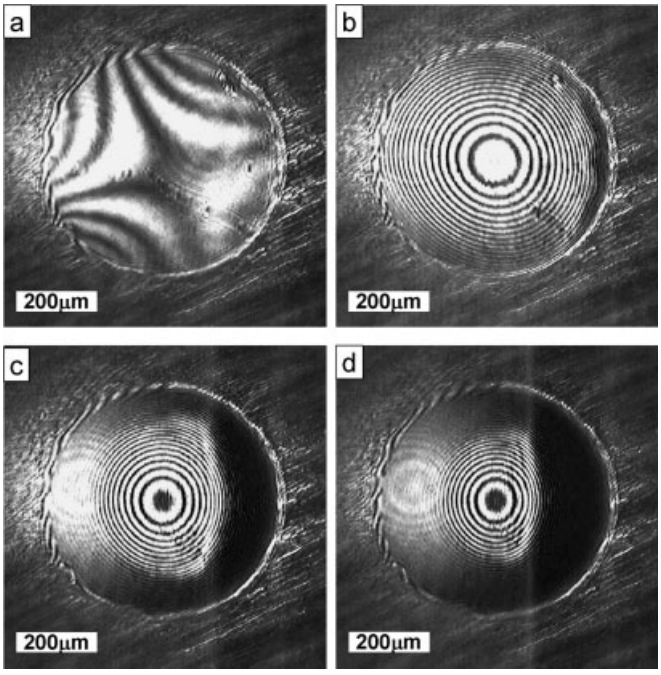

Figure 7. Optical images of a freely suspended 9G9 membrane, 600 μm in diameter, with variable interference patterns observed at different overpressures: a) resting state, no pressure applied; b) 98 Pa; c) 196 Pa; and d) 294 Pa. The increasing number and decreasing spacing of Newton rings are clearly visible.

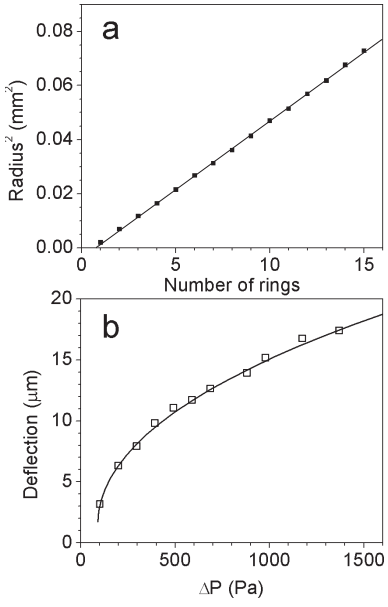

Figure 8. a) Plot of Newton-ring radius versus the number of the interference rings, which obeys a quadratic law indicating an ideal semispherical shape. b) The membrane deflection at different overpressures and the fit of the membrane deformation using Equation 2 as the theoretical model of the elastic plate.

semispherical shape of the membranes under uniform pressure and can be used to calculate the number of rings under large membrane deflection by linear extrapolation of the ring's radius. Following this method, the number of rings was counted, and the maximum deflection of the membranes was calculated, even for very large deflections. The resulting data from this bulging experiment is the pressure dependence of the membrane's deflection (Fig. 8b). This dependence is highly nonlinear and requires a detailed analysis.

Deflection analysis for elastic membranes with different thicknesses and diameters can be conducted by using a theoretical mechanical model for a circular elastic plate clamped to stiff edges.[40,41] According to this model, the general membrane behavior is described by Equation 2[41]

$$P = P_0 + \left[C_0 \frac{E}{1-\nu^2}\frac{h^4}{a^4} + C_1 \frac{\sigma_0 h^2}{a^2}\right]\left(\frac{d}{h}\right) + C_2 \frac{E}{1-\nu}\frac{h^4}{a^4}\left(\frac{d}{h}\right)^3 \quad (2)$$

where P is the overpressure, P_0 is the initial pressure, d is the deflection of the membrane center, and σ_0 is the residual stress. The coefficients C_0, C_1, and C_2 depend upon the geometric shape of the membrane, as tabulated by Poilane et al.[41] The first term corresponds to the initial pressure related to the very small membrane deflection. The second term describes a linear bending regime and includes the residual stresses usually generated by the membrane fabrication. The third term describes the membrane regime of deformation that includes internal stresses within the highly deflected film. As is clear from this equation, for very small deflections, $d \ll h$, the third term is negligible and pressure variation should produce a linear deflection. In contrast, for large deflections, $d \gg h$, the third term becomes dominant and the pressure–deflection relationship should follow a cubic law.

The membrane behavior for a wide range of pressures and for all diameters can be fitted well using Equation 2, with a predominant cubic-term contribution—as expected for these regimes where d (several micrometers) is much larger than h (below one-hundred nanometers) (Figs. 8b,9a). The elastic moduli calculated from the fitting of the experimental data were in range 5.7–9.6 GPa for different membranes and testing procedures (Table 1). Considering the relatively large standard deviation caused by variable fabrication and transfer conditions, we can conclude that the elastic modulus of membranes with different diameters is relatively high and remains virtually constant. The level of the residual stress caused by the membrane pre-stretching after transfer to the solid substrate and complete film drying varies significantly from film to film, as indicated by large deviations, and was within 10–20 MPa for most of the membranes studied here (Table 1). This phenomenon is very common for thin polymer films and is attributed to their shrinkage after transfer in a semi-dry state onto a metal substrate.[42] The maximum deflection observed for the largest membranes before fracture reached 30–40 μm. The loading and unloading cycles were repeated multiple times for the same membrane to test their elastic behavior for relatively small deflections (below 10 μm; Fig. 9b). All loading and unloading curves, repeated for many cycles, almost completely overlapped and followed a cubic law with unchanged parameters, indicating the full reversibility of the membrane deformations.

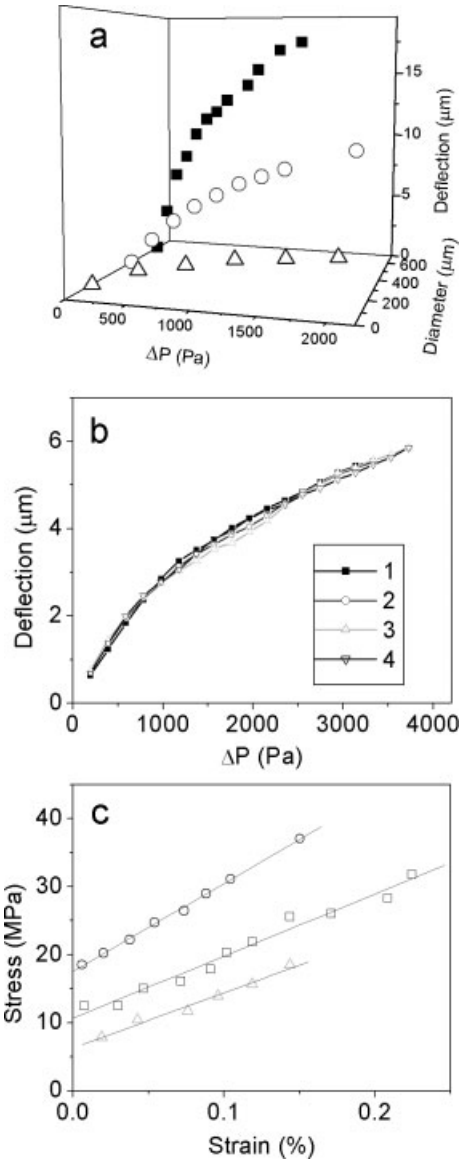

Figure 9. a) The pressure-controlled deflection of freely suspended membranes with different diameters: ■ 600 μm; ○ 400 μm; △ 150 μm. Data reprinted from [26] with permission. b) Pressure-controlled deflection of the freely suspended 9G9 nanomembrane, 400 μm in diameter, obtained repeatedly for several loading–unloading cycles: 1 loading; 2 unloading; 3 loading; and 4 unloading. c) Stress–strain plots for the freely suspended membranes with different diameters and corresponding linear fits: □ 600 μm; ○ 400 μm; △ 150 μm.

Further analysis of the micromechanical properties could be conducted by retrieving the stress–strain data from the pressure–deflection measurements, according to the usual approach for converting experimental parameters, Equation 3[38]

$$\sigma = \frac{P a^2}{4 h d} \quad \text{and} \quad \varepsilon = \frac{2 d^2}{3 a^2} \tag{3}$$

where σ is the stress and ε is the strain, defined in the usual manner for tensile experiments. In this approach, the elastic modulus can be derived as the slope of the initial linear part of the stress–strain curves, which corresponds to the reversible elastic deformation of the material. On the other hand, the elongation to the breaking point and the ultimate strength can be estimated from the data for the highest membrane deflections.

For all membranes, stress–strain curves were fairly linear for small deflections for modest strains $\varepsilon < 0.3$ % generated in the pressure range up to 4 kPa ($d < 20$ μm; Fig. 9c). The elastic moduli estimated using this approach were in the range 5.7–9.0 GPa for different membranes (Table 1). The elongation to the breaking point was usually below 0.8 % for most membranes, reaching 1.5–2 % for membranes with the largest diameter and under lower humidity conditions. The ultimate mechanical strength of these membranes routinely exceeded 50 MPa, with some specimens showing outstanding ultimate strengths of 100 MPa.[25]

The elastic moduli obtained from the stress–strain data are very similar to those obtained from the independent bulging tests (Table 1). Moreover, all sets of values obtained herein for different membranes can be represented by a single value of $E = 7.5 \pm 1.5$ GPa. The statistically higher average value of the elastic modulus derived from the resonance test (13.5 ± 1.5 GPa) is naturally explained by the differences in temporal response of the viscoelastic materials under quasi-static (bulging test) and dynamic (resonance frequency) testing conditions.[37] In fact, the quasi-static elastic moduli were obtained from the deformational data collected using minutes-long loads, unlike the dynamic data for the membranes undergoing deformations with microsecond cycling.

The elastic moduli obtained for the membranes are much higher than the common value for polymeric materials in the glassy state (2–3 GPa).[37] This difference can be accounted for by considering the presence of the gold nanoparticles with a high elastic modulus as a second component of the multiphase nanocomposites. This possible effect can be accounted for in the framework of the Takayanagi model.[43] According to this model, the elastic modulus of a composite material can be calculated as the composite modulus of the components by taking into account their volume fraction and the composite morphology of the membranes. Considering the multilayered structure of the membranes and the stress direction along the membrane surface, we selected the Voight–Kelvin parallel model to evaluate the composite elastic modulus. An elastic modulus of 7.2 GPa was calculated by taking into account the elastic modulus of the gold nanoparticles (78 GPa for bulk gold) and the elastic modulus of glassy polymers ($E = 3$ GPa),[44] see Table 1. This value is close to the average experimental value of the elastic moduli of the membranes estimated from the bulging test and indicates that, in fact, the higher stiffness of the membranes is caused by the presence of the small fraction of gold nanoparticles. In addition, we found that the elastic modulus of 7G7 is slightly higher than that of 9G9. This is consistent with the theoretical results predicted using the Takayanagi model, as the gold-nanoparticle fraction is higher in 7G7 than in 9G9. Moreover, the corresponding measurements of pure, polymeric LbL nanomembranes without gold nanoparticles showed elastic moduli below 2 GPa,[26] indicating the glassy state of the polymer multilayers and additionally confirming that filler

ADVANCED FUNCTIONAL MATERIALS

toughening is the key reason for the high elastic moduli of the nanocomposite membranes.

The glassy state of the SALbL membrane is expected, due to the fact that both polymers used in the bulk state have relatively high glass-transition temperatures (160–190 °C) although some effect of the minimal film thickness should be considered in future studies. The preservation of the glassy state can be associated with the membrane in a dry, freely suspended, and solvent-free state. In fact, several reports on the measurements of the mechanical properties of polyelectrolyte films have been published. The measurements include osmotic pressure, AFM nanoindentation, interferometry, and direct compression with an AFM tip.[45–47] Several results on the micromechanical behavior of similar LbL membranes are consistent with our conclusions, with elastic moduli in the range of 1–2 GPa. However, LbL elastic moduli of ≈ 0.1–200 MPa have also been reported in several studies of microcapsules and thick LbL films on solid supports. Besides some technical issues, such as the use of uncalibrated AFM tips with unknown tip radii,[47] the most probable reasons for a low value of the apparent elastic modulus of an LbL membrane are its swelling in a fluid environment (water is a good solvent for these polyelectrolytes) and significant membrane deformations, as indicated in a recent review on this subject:[48] all these factors were avoided in our study.

Finally, it is well known that polyelectrolyte LbL multilayers adsorb water during fabrication and under ambient conditions during characterization.[23,49] We found that, under high humidity, our SALbL fabrication was less successful, with frequent film fractures observed. In addition, the elastic modulus measured under normal lab conditions (humidity variation of 25–50 % in our clean-room) can be varied within 30–40 % from the average value for membranes measured at different times. Despite this, the nanoscale membranes are quite stable and can be kept on the shelf for several months.

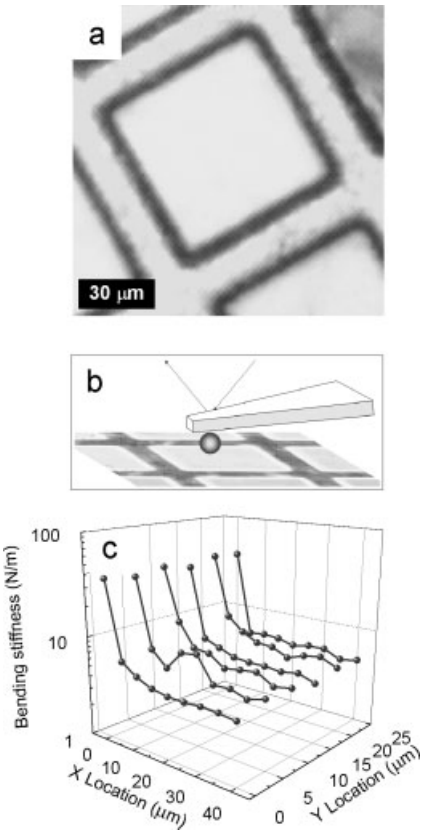

Figure 10. a) Optical microscope image of a freely suspended membrane on a TEM grid with a cell size of 85 μm × 85 μm. b) Schematic of the nanomechanical probing of the freely suspended membrane with the AFM cantilever and attached microsphere. Reprinted from [26] with permission. c) Three-dimensional data of the bending stiffness of the freely suspended membrane within a single TEM grid cell.

2.5. Nanomechanical Membrane Properties Probed via Atomic Force Microscopy

Previous tests have revealed micromechanical properties of membranes either at high frequencies or large deflections. Alternatively, the nanoscale deformation of the freely suspended membranes under the point load can be measured directly for the membranes on a TEM grid with a cell size of 85 μm × 85 μm (Fig. 10a). We applied the colloidal probe mode, whereby the AFM tip is replaced with a microscopic glass ball 2.5 μm in diameter (Fig. 10b).[50] In this experiment, a two-dimensional array of the force–distance curves (cantilever deflection vs. a normal point load) was collected from the edge to the center of one TEM grid. The bending stiffness of the membrane was calculated at these points from the preliminary calibrated cantilever spring constants and deflections according to the usual spring-against-spring approach (Fig. 10c).[51] From the collection of the force–distance curves obtained, we can conclude that a low bending stiffness of the freely suspended membranes was consistently observed over the entire surface area, with a sharp rise in stiffness detected in the vicinity of the grid edges.

To probe the central portion of the membrane, we limited the threshold to obtain maximum membrane deflection below 50 nm (Fig. 11a). The data obtained gives a good illustration of the uniformity of the membrane deformation far from the edges, with maximum deflection close to 30 nm under a normal force below 150 nN. The similarity of the overall shape of the force–distance curves confirms the uniformity of the elastic properties (Fig. 11b). Modest adhesion between the glass ball and the membrane was observed, as indicated by the small hysteresis in the retracing portion of the force–distance curves. The loading curves for the membranes (deflection versus normal load) derived from the force–distance data were very linear for deformations below 40 nm, unlike the large deflections discussed above (compare Figs. 8b,11c). This is consistent with the expectations from the theoretical model predicting a dominance of the bending regime for deflections smaller than the membrane thickness, which is true for this probing regime (see Eq. 2).[36,39,41]

A decrease in the maximum deflection and increase in the bending stiffness were detected at distances of 5–10 μm from the grid edges, due to the glass ball interacting with the stiff copper grid. Very small deflections of the membranes along the edges (below 2 nm) were due to the indentation of the membrane on the stiff substrate (Fig. 11a). The loading curves

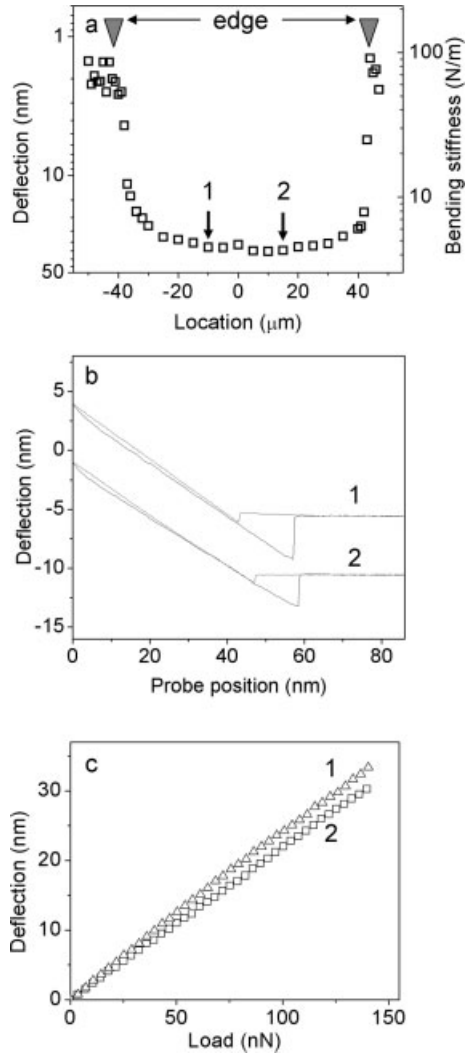

Figure 11. The nanomechanical probing of a freely suspended membrane with an AFM colloidal probe: a) the deflection and the bending constant of the central portion of the freely suspended membrane between the grid edges (85 μm). Arrows mark the locations for which the force–distance curves shown in (b) were collected. b) Experimental force–distance curves for two different locations. c) The loading curves on the freely suspended membrane derived from the AFM data for the two different locations. Reprinted from [26] with permission.

on the edges were analyzed in the framework of the Hertzian approach discussed earlier for the AFM probing,[52–54] in order to evaluate the elastic modulus of the membrane and to verify independently the elastic modulus obtained from the bulging test. The value of this modulus was found to be in the range of 1–2 GPa, which is consistent with the values expected for these glassy polymers.

2.6. Limits of Sensitivity of the Freely Suspended Membranes

To summarize our results on the investigation of the micromechanical properties of nanocomposite membranes, we have combined all the experimental data on micromechanical behavior in a single plot representing the integrated properties of these membranes as prospective, highly sensitive, micromechanical sensing elements (Fig. 12). This double-logarithmic plot represents the relationship of the measurable relative variations of pressure (equivalent to the temperature variation for the isobaric regime) with the corresponding membrane deflection. The experimental data combined on this plot include two different types of bulging testing for small and large deflections, as well as the AFM data renormalized from the point load to the uniform load. All these independent data, for a very broad range of deflections (spanning over three orders of magnitude) and pressures (covering over eight orders of magnitude), give two independent log–log linear relationship (with slopes of 1 and 3 for the nanoscale, $d < h$, and microscale, $d \gg h$, deflections, respectively; Fig. 12). This non-monotonic relationship between pressure and deflection can be well justified with the theoretical model described by Equation 2.

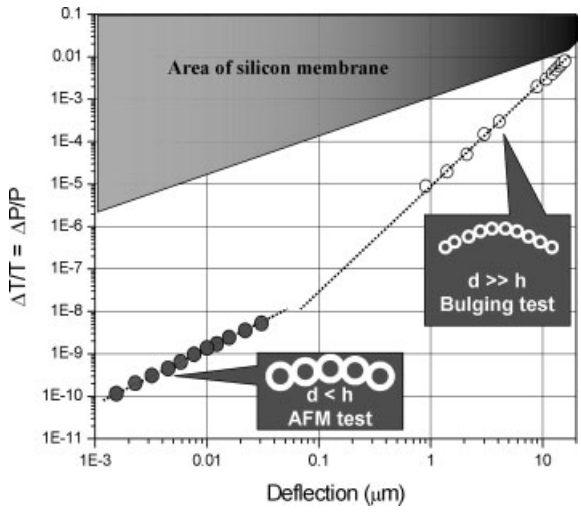

Figure 12. The pressure–temperature variation of deflection of the freely suspended nanocomposite 9G9 membrane, 600 μm in diameter, in comparison with a hypothetical silicon membrane of the same diameter. The results include two independent bulging test data sets for microscale deflections and the AFM data for the nanoscale deflections. The insets are cartoons of the deflected membrane in different regions: low deformation (left) and high deformation (right). Reprinted from [26] with permission.

The extremely high pressure sensitivity of these membranes, down to 10^{-10} for detectable deflections below 2 nm, is apparent from this plot. This sensitivity limit is two to three orders of magnitude below the threshold hearing of a human ear.[55] Comparison with the theoretical estimate of the sensitivity of the hypothetical silicon membrane of the same diameter—derived from Yamashita estimates for microthermal sensors[9]—(gray area) shows that the pressure and thermal sensitivity of the compliant nanocomposite membranes fabricated here is three to four orders of magnitude higher. Moreover, as we estimated from temperature-equivalent variations ($\Delta T/T = \Delta P/P$ under isochoric conditions, which is justified for our experiments), these membranes can also be two to three orders of

magnitude more sensitive than the existing, uncooled thermal sensors based on microcantilever technology with a theoretical lowest limit of detectable temperature variations well below 1 mK.[56]

3. Conclusion

We fabricated freely suspended, nanocomposite LbL membranes with a multilayered, polymer–nanoparticle structure that demonstrated outstanding micromechanical properties and a record sensitivity to pressure (temperature) variations. These unique nanomembranes possess very stable micromechanical characteristics and a sensitivity far surpassing any existing pressure sensors based on stiff inorganic materials with large lateral dimensions, as well as the human ear with its flexible biological membrane. We believe that these nanocomposite membranes, with microscopic lateral dimensions, are outstanding candidates for the next generation of acoustic and thermal microscopic sensor arrays of exceptional sensitivity.

4. Experimental

Materials: PSS (weight-average molecular weight, $M_W = 70\,000$) and PAH ($M_W = 65\,000$) were purchased from Aldrich and used as received without further purification. Ultrapure water was obtained using a Nanopure system (resistivity 18 MΩ cm) and used in all experiments. Silicon wafers of {100} orientation with one polished side (Semiconductor Processing Co.) were atomically smooth. Silicon wafers, cut to a typical size of 10 mm × 20 mm, were cleaned in fresh piranha solution [1:3 (vol./vol.) H_2O_2/H_2SO_4] according to the usual procedure adopted in our laboratory [57]. *Attention: piranha solution is extremely dangerous and should be handled with great care*. After cleaning, the substrates were rinsed thoroughly with Nanopure water.

Synthesis of Gold Nanoparticles: Gold nanoparticles with an average diameter of 12.7 nm were prepared according to the literature procedure [58]. Initially, sodium citrate solution (5 mL, 1 wt.-%) was quickly injected into a solution of boiling $HAuCl_4$ (1 mM, 50 mL). The (continuously stirred) solution was boiled for 10 min. The heating was then discontinued, and the solution was stirred for an additional 15 min. The gold-nanoparticle solution was kept in a dark, dry area at room temperature and was used within 3–4 weeks of synthesis.

Fabrication of Freely Suspended Membranes: A sacrificial CA layer was spin-coated on the freshly cleaned silicon substrate. A droplet (150 μL) of CA acetone solution (1 wt.-%) was dropped onto the silicon substrate and rotated for 20 s at 3000 rpm (rpm: revolutions per minute). Multilayer films with different thicknesses (general formula: $(PAH/PSS)_n PAH/Au/(PAH/PSS)_n/PAH$) were deposited using the well-known SALbL method [24,25,27,28]. During the course of SALbL fabrication, a droplet (150 μL) of the PAH solution (0.2 wt.-%) was dropped on the substrate and rotated for 20 s at 3000 rpm. The substrate was rinsed twice with Nanopure water and dried while spinning for 30 s. In the same manner, PSS solution (0.2 wt.-%) was deposited after drying. This procedure was repeated several times until the necessary number of polymer bilayers n was achieved. To form the central layer, a droplet (150 μL) of the gold-nanoparticle solution was dropped onto the substrate and left for 30 min. Then, the substrate was rinsed twice with Nanopure water and the same number of polymer bilayers n was then deposited on the top.

Acetone was used to dissolve the sacrificial CA layer and release the membrane from the silicone substrate. After that, freely suspended membranes were picked up by the different substrates. To lift the membrane, we used either a highly polished copper plate (Electron Microscopy Sciences) with a single hole (different sized holes were used), clean silicon wafers, or copper TEM grids.

TEM Imaging: Freely suspended nanomembranes were picked up onto a 200-mesh copper grid and dried overnight before TEM investigation. A Phillips CM30 electron microscope with a LaB_6 filament was used, and it was operated at 300 kV. The nanomembranes were very stable under high vacuum and the gold nanoparticles in the membrane were clearly observed.

AFM Measurements: AFM topographical and phase images were collected with a Dimension 3000 AFM microscope (Digital Instruments) in the tapping mode according to the usual procedure adapted in our laboratory for ultrathin polymer films [59]. Silicon tips with a spring constant of 50 N m^{-1} were used for all scans. The radii of the tips were in the range of 20–40 nm, as calculated from the profiles of the reference gold-nanoparticle standards [60]. AFM images were obtained for different scan sizes from 1 to 20 μm, at a scanning rate of 1 Hz. To obtain a film thickness, the freely suspended membrane was picked up on the silicon wafer and its edge area was scanned. The film thickness and the surface microroughness were obtained from a bearing analysis of the scanned areas.

Point-Load AFM Measurements: Point-load measurements were made with the Dimension 3000 AFM microscope on a freely suspended membrane on a 200-mesh copper grid (cell size of 85 μm × 85 μm; Ted Pella, Inc). The silicon cantilevers used for this testing had a spring constant of 14.0 ± 2.8 N m^{-1}, as measured with the spring-against-spring technique [61]. In this method, a silicon cantilever with a known spring constant was deflected by a cantilever with unknown spring constant, and data for the force–distance curve was received. From this curve, the unknown spring constant was obtained using a simple double-spring model. The borosilicate-glass particles, 2.5 μm in diameter, attached to the end of the cantilever were used for these experiments (Novascan Technology).

Bulging Test: The bulging test was conducted by applying a hydrostatic pressure from one side of a membrane covering a copper plate with a single hole. The hole diameter varied from 150 to 600μm. The pressure was obtained by measuring the height difference of a water column in a U-shaped glass tube. The pressure was measured with precision, ± 0.05 cm of the water column, which corresponds to 4.9 Pa. The membrane deflection was measured by a custom-built interference optical set-up with a helium–neon laser (wavelength 632.8 nm). The optical images, with variable Newton rings under different pressures, were recorded by a charge-coupled device (CCD) camera. The deflection of the top of the membrane was calculated by determining the average spacing from one-dimensional Fourier transforms and calculating the number of the rings, considering that the distance Z between the neighboring rings corresponds to a half of the wavelength.

Received: April 7, 2004
Final version: July 2, 2004

[1] W. S. Trimmer, *Micromechanics and MEMS: Classic and Seminar Papers to 1990*, IEEE Press, New York **1996**.
[2] J. W. Choi, C. H. Ahn, S. Bhansali, H. T. Henderson, *Sens. Actuators B* **2000**, *68*, 34.
[3] L. Lofdahl, M. Gad-el-Hak, *Meas. Sci. Technol.* **1999**, *10*, 665.
[4] R. S. Muller, in *Micro/Nanotribology and Its Applications* (Ed: B. Bhushan), Kluwer Press, Dordrecht, The Netherlands **1997**, p. 579.
[5] V. V. Tsukruk, *Adv. Mater.* **2001**, *13*, 95.
[6] I. Luzinov, S. Minko, V. V. Tsukruk, *Prog. Polym. Sci.* **2004**, *29*, 635.
[7] E. Defay, C. Millon, C. Malhaire, D. Barbier, *Sens. Actuators A* **2002**, *99*, 64.
[8] F. Hedrich, S. Billat, W. Lang, *Sens. Actuators A* **2000**, *84*, 315.
[9] K. Yamashita, A. Murata, M. Okuyama, Sens. *Actuators A* **1998**, *66*, 29.
[10] D. R. Lee, K. Shin, O. H. Seeck, H. Kim, Y.-S. Seo, M. Tolan, M. H. Rafailovich, J. Sokolov, S. K. Sinha, *Phys. Rev. Lett.* **2003**, *90*, 185 503.
[11] N. Cuvillier, V. Petkova, M. Nedyalkov, F. Millet, J.-J. Benattar, *Phys. B (Amsterdam, Neth.)* **2000**, *238*, 1.

[12] S. V. Yablonskii, K. Nakano, A. S. Mikhailov, M. Ozaki, K. Yoshino, *Jpn. J. Appl. Phys. Part 1* **2003**, *42*, 198.
[13] W. A. Goedel, R. Heger, *Langmuir* **1998**, *14*, 3470.
[14] F. Mallwitz, W. A. Goedel, *Angew. Chem. Int. Ed.* **2001**, *40*, 2645.
[15] M. H. Lim, D. G. Ast, *Adv. Mater.* **2001**, *13*, 718.
[16] Y. Lvov, G. Decher, H. Moehwald, *Langmuir* **1993**, *9*, 481.
[17] V. V. Tsukruk, *Adv Mater.* **1998**, *10*, 253.
[18] G. Decher, *Science* **1997**, *277*, 1232.
[19] V. V. Tsukruk, *Prog. Polym. Sci.* **1997**, *22*, 247.
[20] V. V. Tsukruk, F. Rinderspacher, V. N. Bliznyuk, *Langmuir* **1997**, *13*, 2171.
[21] V. V. Tsukruk, V. N. Bliznyuk, D. W. Visser, A. L. Campbell, T. Bunning, W. W. Adams, *Macromolecules* **1997**, *30*, 6615.
[22] A. A. Mamedov, N. A. Kotov, *Langmuir* **2000**, *16*, 5530.
[23] A. A. Mamedov, N. A. Kotov, V. Prato, D. M. Guldi, J. P. Wicksted, A. Hirsch, *Nat. Mater.* **2002**, *1*, 190.
[24] C. Jiang, S. Markutsya, V. V. Tsukruk, *Langmuir* **2004**, *20*, 882.
[25] C. Jiang, S. Markutsya, V. V. Tsukruk, *Adv. Mater.* **2004**, *16*, 157.
[26] C. Jiang, S. Markutsya, Yu. Pikus, V. V. Tsukruk, *Nat. Mater.* **2004**, *3*, 721.
[27] J. Cho, K. Char, J.-D. Hong, K.-B. Lee, *Adv. Mater.* **2001**, *13*, 1076.
[28] P. A. Chiarelli, M. S. Johal, J. L. Casson, J. B. Roberts, J. M. Robinson, H.-L. Wang, *Adv. Mater.* **2001**, *13*, 1167.
[29] P. H. Walker, J. G. Tompson, *Proc. Am. Soc. Test. Mater.* **1922**, *22*, 464.
[30] *Multilayer Thin Films* (Eds: G. Decher, J. B. Schlenoff), Wiley-VCH, Weinheim, Germany **2003**.
[31] H. Y. Bae, G. M. Choi, *Sens. Actuators B* **1999**, *55*, 47.
[32] Y. Shi, J. Liu, Y. Yang, *J. Appl. Phys.* **2000**, *87*, 4254.
[33] S. Zhou, *The Resonator Handbook*, National Technical Information Service, Springfield, VA **1993**.
[34] H. H. Kim, B. K. Ju, Y. H. Lee, S. H. Lee, J. K. Lee, S. W. Kim, *Microelectron. Reliab.* **2004**, *44*, 237.
[35] F. Ayela, T. Fouinier, J. Chaussy, *Sens. Actuators A* **1997**, *61*, 339.
[36] S. Timoshenko, *Theory of Plates and Shells*, 2nd ed., McGraw-Hill Book Company, New York **1959**.
[37] L. H. Sperling, *Introduction to Physical Polymer Science*, 3rd ed., Wiley, New York **2001**.
[38] J. W. Beams, in *Structure and Properties of Thin Solid Films*, (Eds: C. A. Neugebauer, J. B. Newkirk, D. A. Vermilyea), John Wiley, New York **1959**, p. 183.
[39] J. J. Vlasak, W. D. Nix, *J. Mater. Res.* **1992**, *7*, 3242.
[40] S. Jayaraman, R. L. Edwards, K. J. Hemker, *J. Mater. Res.* **1999**, *14*, 688.
[41] C. Poilane, P. Delobelle, C. Lexcellent, S. Hayashi, H. Tobushi, *Thin Solid Film* **2000**, *379*, 156.
[42] L. F. Francis, A. V. McCormick, D. M. Vaessen, J. A. Payne, *J. Mater. Sci.* **2002**, *37*, 4717.
[43] L. H. Sperling, *Polymeric Multicomponent Materials*, Wiley, New York **1997**.
[44] J. F. Rudd, E. F. Gurnee, *J. Appl. Phys.* **1957**, *28*, 1096.
[45] a) C. Gao, S. Leporatti, S. Moya, E. Donath, H. Moehwald, *Langmuir* **2001**, *17*, 3491. b) F. Dubreuil, N. Elsner, A. Fery, *Eur. Phys. J. E* **2003**, *12*, 215.
[46] O. I. Vingradova, D. Andrienko, V. V. Lulevich, S. Nordschild, G. B. Sukhorukov, *Macromolecules* **2004**, *37*, 1113.
[47] O. Mermut, J. Lefebvre, D. G. Gray, C. J. Barrett, *Macromolecules* **2003**, *36*, 8819.
[48] A. Fery, F. Dubreuil, H. Moehwald, *New J. Phys.* **2004**, *6*, 18.
[49] B. D. Vogt, C. L. Soles, H. Lee, E. K. Lin, W. Wu, *Langmuir* **2004**, *20*, 1453.
[50] S. Zauscher, D. J. Klingenberg, *J. Colloid Interface Sci.* **2000**, *229*, 497.
[51] V. V. Tsukruk, V. V. Gorbunov, *Probe Microsc.* **2002**, *3*, 241.
[52] S. A. Chizhik, Z. Huang, V. V. Gorbunov, N. K. Myshkin, V. V. Tsukruk, *Langmuir* **1998**, *14*, 2606.
[53] V. V. Tsukruk, Z. Huang, S. A. Chizhik, V. V. Gorbunov, *J. Mater. Sci.* **1998**, *33*, 4905.
[54] a) A. Kovalev, H. Shulha, M. LeMieux, N. Myshkin, V. V. Tsukruk, *J.Mater. Res.* **2004**, *19*, 716. b) H. Shulha, A. Kovalev, N. Myshkin, V. V. Tsukruk, *Eur. Polym. J.* **2004**, *40*, 949. c) M. LeMieux, S. Minko, D. Usov, M. Stamm, V. V. Tsukruk, *Langmuir* **2003**, *19*, 6126. d) M. LeMieux, D. Usov, S. Minko, M. Stamm, H. Shulha, V. V. Tsukruk, *Macromolecules* **2003**, *36*, 7244. e) V. V. Tsukruk, H. Shulha, X. Zhai, *Appl. Phys. Lett.* **2003**, *82*, 907.
[55] J. Weng, K. Y. Guentchev, *J. Acoust. Soc. Am.* **2001**, *110*, 310.
[56] A. Rogalski, *Prog. Quantum Electron.* **2003**, *27*, 59.
[57] V. V. Tsukruk, V. N. Bliznyuk, *Langmuir* **1998**, *14*, 446.
[58] K. C. Grabar, R. G. Freeman, M. B. Hommer, M. J. Natan, *Anal. Chem.* **1995**, *67*, 735.
[59] a) V. V. Tsukruk, D. H. Reneker, *Polymer* **1995**, *36*, 1791. b) V. V. Tsukruk, *Rubber Chem. Technol.* **1997**, *70*, 430. c) *Scanning Probe Microscopy of Polymers*, ACS Symposium Series, Vol. 694, American Chemical Society, Washington, DC **1998**.
[60] J. Vesenka, S. Manne, R. Giberson, T. Marsh, R. Henderson, *Biophys. J.* **1993**, *65*, 992.
[61] a) J. L. Hazel, V. V. Tsukruk, *J. Tribol.* **1998**, *120*, 814. b) J. L. Hazel, V. V. Tsukruk, *Thin Solid Films* **1999**, *339*, 249.

